Appl Phys A (2011) 105:17–23
DOI 10.1007/s00339-011-6540-8

Applied Physics A
Materials Science & Processing

RAPID COMMUNICATION

Ablation of polymers by focused EUV radiation from a table-top laser-produced plasma source

Frank Barkusky · Armin Bayer · Klaus Mann

Received: 7 June 2011 / Accepted: 6 July 2011 / Published online: 6 August 2011

Abstract We have investigated ablation of polymers with radiation of 13.5 nm wavelength, using a table-top laser produced plasma source based on solid gold as target material. A Schwarzschild objective with Mo/Si multilayer coatings was adapted to the source, generating an EUV spot of 5 µm diameter with a maximum energy density of ∼1.3 J/cm^2. In combination with a Zirconium transmission filter, radiation of high spectral purity (2% bandwidth) can be provided on the irradiated spot. Ablation experiments were performed on PMMA, PTFE and PC. Ablation rates were determined for varying fluences using atomic force microscopy and white light interferometry. The slopes of these curves are discussed with respect to the chemical structure of the polymers. Additionally, the ablation behavior in terms of effective penetration depths, threshold fluences and incubation effects is compared to literature data for higher UV wavelength.

1 Introduction

Laser ablation and photo-etching of polymers have been studied extensively especially in the visible and deep ultraviolet (DUV) spectral range [1–5]. For these wavelengths, ablation can be described in terms of thermal, photo-thermal and photo-chemical models, or as a combination of these mechanisms [6]. From a practical point of view, a structuring process based on photochemistry is preferable, since the absence of thermal influences leads to smoother profiles with less debris, accomplishing higher spatial resolution and smaller structure sizes. A prerequisite for a predominant photochemical process without thermal load is short wavelength radiation with photon energies high enough to directly break the polymer bonds [6]. Furthermore, taking the Rayleigh criterion into account, the use of short wavelength radiation increases the theoretical resolution of optics, accomplishing the direct generation of feature sizes below 100 nm [7].

The interaction of radiation with a wavelength lower than 157 nm with various polymers was investigated in a number of publications up to now. Examples are the structuring of PMMA using a capillary discharge Ne-like Ar laser (wavelength 46.9 nm, pulse duration 1.2 ns) [8], the free-electron laser (FEL) in Hamburg (FLASH) emitting EUV radiation at a pulse duration of 25 fs [9], and a zinc x-ray laser (wavelength 21 nm, pulse duration 90 ps) [10]. In this context it is interesting to note that at the FLASH light source the ablation of PMMA is used also for spatial characterization of the FEL beam.

Many experiments were performed using synchrotron sources, investigating the influence of low energy density EUV radiation on polymers like PMMA [11–13] or PTFE [14–16]. In the last years also table-top EUV sources [17, 18] were used for structuring of polymers. Using a laser-induced Ta plasma in combination with a grazing incidence Au covered collector mirror an energy density of up to 0.3 J/cm^2 was obtained that could be applied for ablation of silica glass [19]. Unfortunately, grazing incidence mirrors are not useful for mask-projection due to their inherently low numerical aperture and corresponding low spatial resolution.

In this paper, we present a table-top EUV setup which is able to generate energy densities up to 1.3 J/cm^2 at pulse durations of 8.8 ns with high spectral purity. It consists of a laser-produced plasma based on a solid gold target. The

F. Barkusky (✉) · A. Bayer · K. Mann
Laser-Laboratorium-Göttingen e.V., Hans-Adolf-Krebs-Weg 1, 37077 Göttingen, Germany
e-mail: frank.barkusky@llg-ev.de

EUV radiation is focused by a modified Schwarzschild objective, consisting of two spherical Mo/Si multilayer mirrors. The spectral filtering of incident radiation by the Mo/Si mirrors (bandwidth ∼2% @ 13.5 nm) in combination with a zirconium foil for blocking non-EUV radiation ($T_{20\ \mathrm{nm}-3000\ \mathrm{nm}} < 1\%$) ensures that all observed effects can be attributed to 13.5 nm radiation exclusively. The resolution of the objective is roughly 130 nm [20].

We present investigations on the direct photo-etching behavior of various polymers under intense spectrally pure EUV radiation. Etch depths for different pulse numbers and energy densities are measured by atomic force microscopy. The resulting etch rates and calculated attenuation lengths are discussed with respect to the chemical structure of the polymers and compared with respective data from excimer laser ablation studies. Furthermore, the roughness of the etched profiles was determined and compared to the non-irradiated polymer surface, indicating a smooth ablation process independent from the applied EUV energy density.

2 Experimental setup

The experimental setup consists of a laser-based EUV/XUV source and a separate optics chamber adapted to this source (cf. Fig. 1) [21–23]. EUV radiation is generated by focusing a Nd:YAG laser (Innolas, wavelength 1064 nm, maximum pulse energy 700 mJ, pulse duration 8.8 ns) onto gaseous or solid targets [26, 28]. For small EUV plasmas with high brilliance, a solid Au target (200 µm thick Au foil fixed on a copper rod) is used, yielding a plasma diameter of ∼50 µm (FWHM).

In order to achieve high EUV fluences, a Schwarzschild objective with a demagnification of 9.8× at a maximum numerical aperture of 0.4 was employed [24]. It consists of two spherical, annular mirror substrates coated with a Mo/Si multilayer system (reflectivity $R \sim 0.65$ per mirror at 13.5 nm). A plane mirror (Au coated silicon wafer, $R \sim 0.675$ for grazing angle of 10 degree [25]) is positioned between source and objective in order to protect the Mo/Si multilayers against contamination from debris of the laser plasma. Due to a significant reflectivity of the Mo/Si mirrors also at wavelengths above 100 nm, a 200 nm thick zirconium foil fixed on an etched steel mesh was inserted in the beam path, blocking effectively all radiation above 25 nm [25].

Table 1 compiles selected properties of the employed EUV source and optics system as used in the experiments. The plasma diameter was measured by direct photo-etching of PMMA at low fluences (below 500 mJ/cm^2). Here, the depth per pulse is linear to the incident EUV energy density [26]. Hence, the intensity distribution in the focus of the Schwarzschild objective is proportional to the depth profile of the ablation crater and can be easily determined from AFM-images. The integrated EUV energy in the focus was measured with a photodiode (AXUV-HS5, manufacturer International Radiation Detectors, Inc.) positioned 200 µm behind the focus of the objective. This diode has a well-defined quantum efficiency, thus the number of EUV photons can be calculated from the photo-induced current, measured with an oscilloscope.

Table 1 Parameters of the laser-based EUV plasma source and optics system, displayed for the image plane of the Schwarzschild objective

Wavelength	13.5 nm (2% bandwidth, FWHM)
Spectral filtering	zirconium + 2x Mo/Si reflections
Pulse duration	∼8.8 ns (FWHM)
Repetition rate	1 Hz
EUV spot size	5.3 µm × 1.72 µm (FWHM)
Irradiated Area	7.16 µm^2
Maximum EUV energy	≤96.7 nJ
Maximum EUV energy density	≤1.35 J/cm^2

Using a spherical laser focus on the gold target, EUV energy density saturates at 0.73 J/cm^2 due to overheating of the plasma by the incoming laser energy. Further enhancement was achieved by use of a line focus rather than a spherical focus on the solid target [27], leading to a maximum EUV fluence of 1.35 J/cm^2.

3 Experimental results

In order to complete and extend the results of previous publications [26, 28], polymethyl methacrylate (PMMA), polytetrafluoroethylen (PTFE) and polycarbonate (PC) were used for ablation experiments. In Fig. 2 chemical formulas of the polymers are displayed.

Polymer plates of 1–3 mm thicknesses (Goodfellow) were cut into 1 cm × 1 cm pieces and cleaned in ethanol using an ultrasonic bath before exposure. Each polymer was irradiated with EUV spots of different EUV energy densities with 1, 5 and ten pulses per site. Maximum depths were measured by atomic force microscopy in tapping mode.

In Fig. 3 (left), the AFM image of PMMA is displayed, irradiated with a single EUV pulse of 1.3 J/cm^2. The observed very smooth surface of the ablated area is typical for the EUV-polymer ablation process presented in this paper. Independent from the investigated polymer, the roughness increases by less than 30% (PMMA: <10% from a RMS value of ∼5.4 nm, measured by AFM on a non-irradiated site of the sample).

In Fig. 3 (right), PMMA crater depths for selected energy densities are displayed as a function of the number of applied EUV pulses. A strong linear dependence between depth and pulse number can be observed. This absence of incubation effects is typical for the investigated polymers

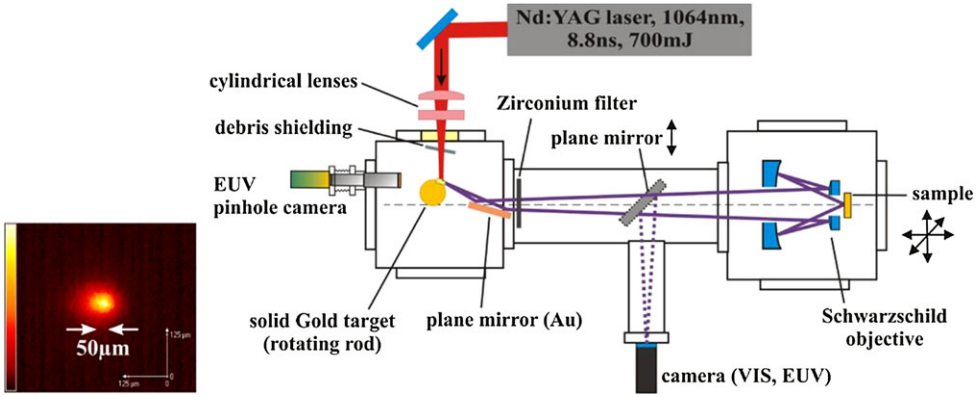

Fig. 1 Schematic drawing of the EUV source and optics system. On the *left* a pinhole camera image of the EUV plasma (solid gold target) is displayed

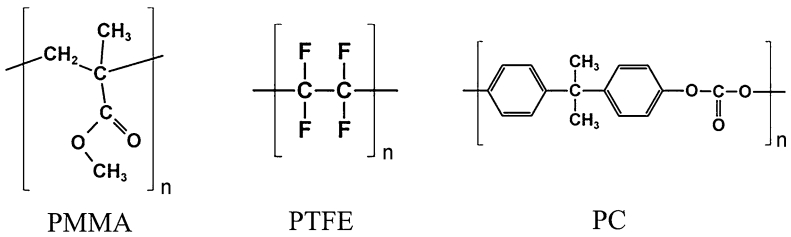

Fig. 2 Structural formula of PMMA, PTFE and PC

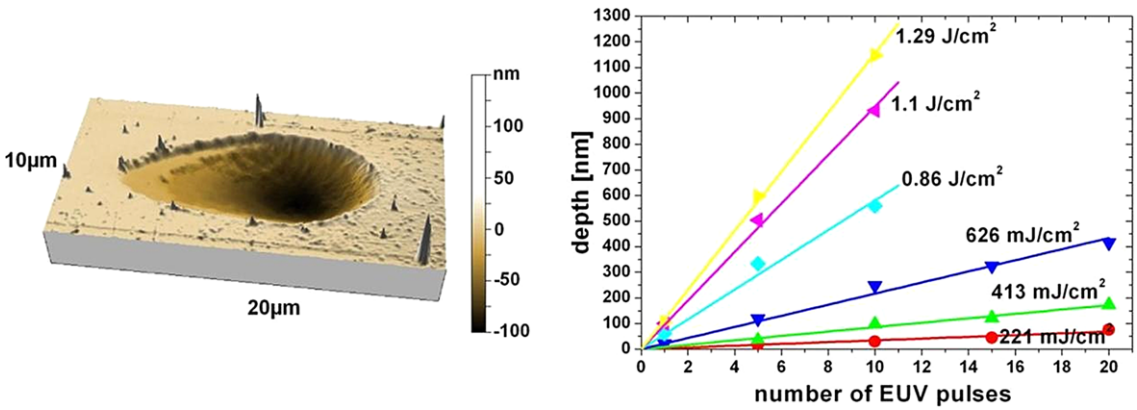

Fig. 3 *Left*: AFM-image of PMMA, structured with one EUV pulse of ~1.3 J/cm^2. *Right*: maximum depths of the profiles, displayed for 1, 5 and 10 EUV pulses per site and selected EUV energy densities

and can be observed for all applied EUV energy densities. From the linear fit of the fluence dependent ablation depths the ablation rates can be determined. For PMMA, these results are displayed in Fig. 4.

For low fluences up to ~500 mJ/cm^2, a linear dependence can be observed with a slope of 0.016 (nm/pulse)/(mJ/cm^2). The absence of a threshold fluence was already shown in previous publications for much lower energy densities down to several mJ/cm^2 [28]. This indicates a photochemically dominated process, where the energy of single photons (~92 eV at 13.5 nm wavelength) is high enough to break the polymer bonds, having binding energies in the range of several eV [30]. Single polymer fragments might be disconnected from the polymer and escape into vacuum, leading to a very low ablation rate per pulse.

For higher fluences above 600 mJ/cm^2 the ablation rate increases dramatically to values of more than 100 nm/pulse. The logarithmic trend of these data can be fitted by (1), resulting from Lambert–Beers law [29]:

$$r = \frac{1}{\alpha_{\text{eff}}} \cdot \ln\left(\frac{H}{H_{\text{th}}}\right) \tag{1}$$

where r denotes the ablation rate, α_{eff} the effective absorption coefficient, H the applied energy density, and H_{th} the threshold energy density for the logarithmic trend. The parameters of the fit are summarized in Table 2, yielding a threshold fluence of 558 mJ/cm^2 for PMMA and an effective penetration depth ($=1/\alpha_{\text{eff}}$) of ~135 nm. The latter is only 25% lower than the tabulated penetration depth of approximately 180 nm [25]. This good correlation is also an

indication for a photochemical process, since the material is removed only from the sample volume in which the incoming radiation is absorbed.

For PTFE and PC the ablation rates were measured in the same way as for PMMA. Results are displayed in Fig. 5, fit parameters are listed in Table 2. Like PMMA, both polymers do not show an energy density threshold for material removal. However, the fluence dependence of the ablation rate is different: In case of PTFE the linear fit for low fluences merges smoothly into the already observed logarithmic trend for higher fluences. The slope of the linear fit curve is 0.099 (nm/pulse)/(mJ/cm^2), which is the highest for the three polymers. From the logarithmic fit for higher fluences (>0.3 mJ/cm^2), an effective penetration depth of 29 nm can be determined, being only ∼40% lower than the tabulated value of ∼50 nm [25]. This low penetration depth compared to PMMA and PC is an indication for a very strong absorption of 13.5 nm radiation, resulting from the high fluorine content in the chemical structure of PTFE (see Fig. 2, [25]). This might also explain the strong increase of the ablation rate at low fluences.

The graph for PC is comparable to PMMA, with a linear range for fluences below 600 mJ/cm^2 and a strongly increasing rate at higher energy densities, showing a logarithmic trend (Fig. 5, right). However, the ablation rates are approximately one order of magnitude smaller than for PMMA, even though the tabulated penetration depths are similar. This results in a huge difference between the effective penetration depth of ∼13 nm, calculated from the logarithmic fit, and the tabulated value of approximately 200 nm. The main reason might be the chemical structure of PC with numerous aromatic rings. This structure protects the polymer from radiation damage. Assuming a predominant photochemical degradation process, a broken aromatic double bond would not lead necessarily to a broken polymer chain. This behavior is already known from experiments in the UV spectral range [31]. The reduced photo-induced fragmenta-

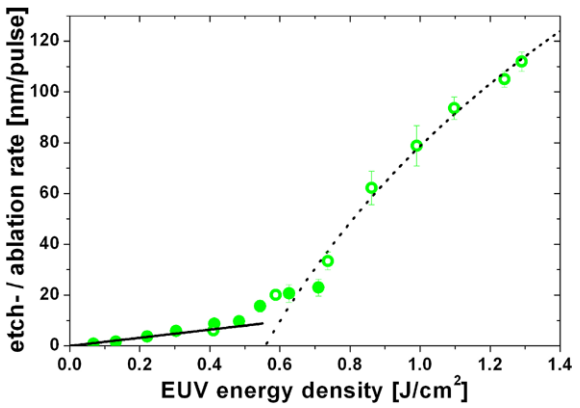

Fig. 4 Ablation rates of PMMA versus EUV energy density: *solid circles*: spherical plasma, *open circles*: elongated plasma, *continuous line*: linear fit for low fluences, *dotted line*: logarithmic fit

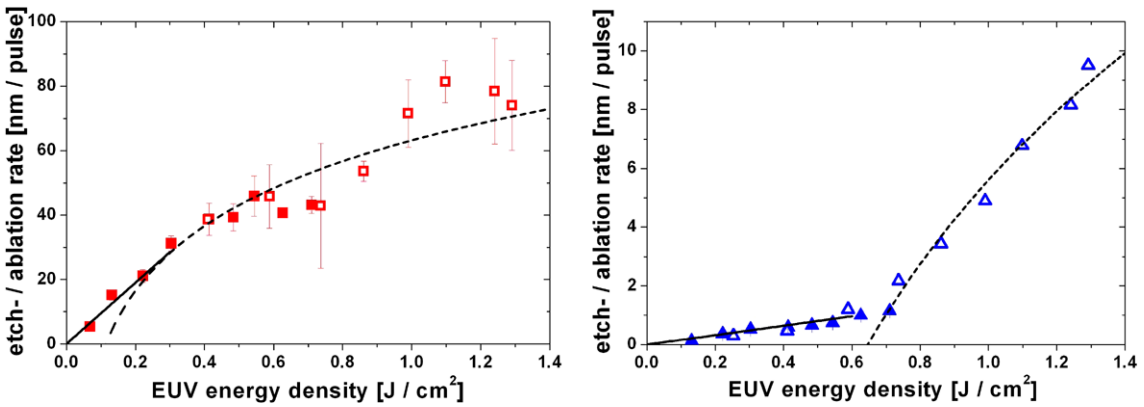

Fig. 5 Ablation rates of PTFE (*left*) and PC (*right*) versus EUV energy density: *solid symbols*: spherical plasma, *empty symbols*: elongated plasma, *continuous line*: line fit for low fluences, *dotted line*: logarithmic fit

Table 2 Fit parameters for PMMA, PTFE and PC as calculated from the ablation rate measurements, including the ablation parameters determined from the logarithmic fit (1)

			PMMA	PTFE	PC
Linear slope (low fluences)	$\mathrm{d}r/\mathrm{d}H$	$\left(\frac{\mathrm{nm/pulse}}{\mathrm{mJ/cm^2}}\right)$	0.016	0.099	0.0015
Tabulated penetration depth [25]	d	(nm)	186–170	52–47	214–196
Effective penetration depth	$d_{\mathrm{eff}} = 1/\alpha_{\mathrm{eff}}$	(nm)	134.7	29	12.9
Ablation threshold	H_{th}	(mJ/cm^2)	558	113.2	646

Table 3 Characteristics of PTFE ablation for EUV radiation (measured) and higher UV wavelengths (from selected publications)

		13.5 nm	46.8 nm [32]	125 nm [33]	157 nm [31, 33]	193 nm [33]
Incubation		No	No	No	–	–
d	(nm)	50	12	–	–	–
$d_{\text{eff}} = 1/\alpha_{\text{eff}}$	(nm)	29	–	0.1	161–172	6660
H_{th}	(mJ/cm^2)	113	–	1	54–80	1600

Table 4 Selected data on PMMA ablation characteristics for EUV radiation (measured) and for higher wavelengths (from selected publications)

		13.5 nm	46.8 nm [32]	125 nm [33]	157 nm [31, 33, 36]	193 nm [36–38, 40]	248 nm [37, 39–41]
Incubation		No	No	No	No	Yes	Yes
d	(nm)	191	19	–	–	2.200–5.000	20.000–154.000
$d_{\text{eff}} = 1/\alpha_{\text{eff}}$	(nm)	135	–	0.15	117	250	–
H_{th}	(mJ/cm^2)	558	–	1	41	80	750

tion of the polymer due to the aromatic groups could lead to higher photo-thermal heating of the material. This would also explain a ring-shaped change in the surface morphology around the irradiated area, as displayed in a previous publication [26].

The parameters determined from the measured ablation curves as well as tabulated penetration depths are compiled in Table 2. Due to the high numerical aperture of the Schwarzschild objective, the incidence angles on the irradiated samples range from 12.7 deg to 26.6 deg. Therefore, the theoretical penetration depths are calculated for the mean angle of ∼20 deg.

4 Comparison with ablation at higher wavelengths

In order to compare the characteristics of the described ablation curves with experiments in the deep and vacuum UV spectral range, corresponding literature data are compiled in Table 3 (PTFE) and Table 4 (PMMA). For comparability, only data for nanosecond pulse durations are displayed.

Apart from femtosecond laser ablation where multiple-photon processes are dominant [34], structuring of PTFE with wavelengths above 193 nm is hardly possible due to the low absorption and/or high penetration depth [35]. For shorter wavelength the absorption increases, whereas the threshold value of the ablation decreases from 1,6 J/cm^2 ($\lambda = 193$ nm) to 1 mJ/cm^2 for $\lambda = 125$ nm. The effective penetration depths, determined from the ablation rates, are reduced accordingly from ∼6.6 µm to 0.1 nm. For even shorter wavelengths the values for effective and tabulated penetration depths are rising again. This change in the absorption mechanism around $\lambda = 125$ nm can be explained by the fact that here the photon energy of ∼10 eV is in the range of the binding energy in the polymer [30]. Therefore, the highest absorption cross-section is observed in this spectral region. With further increasing photon energies, single photons are able to break one or more chemical bonds. Hence, even lowest EUV energy densities are leading to detectable material removal.

A similar behavior can be observed for PMMA, as displayed in Table 4. For the DUV wavelengths of 193 nm and 248 nm incubation effects have been reported, which can be explained by the formation of C=C bonds due to the first UV pulses, enabling an effective absorption of the UV radiation within the polymer [42]. Consequently, the ablation rates are strongly increasing after several pulses, and the effective penetration depth for high pulse numbers is much lower than the tabulated one. For wavelengths below 157 nm no incubation effects can be observed, although C=C bonds are generated during irradiation [26]. However, since the absorption in the EUV wavelength range depends more on the atomic species than on the character of chemical bonds [25], the formation of C=C bonds would not change the absorption behavior of the polymer significantly.

The ablation threshold fluence decreases from $H_{\text{th}} = 750$ mJ/cm^2 ($\lambda = 248$ nm) rapidly to ∼1 mJ/cm^2 at $\lambda = 125$ nm. As already mentioned for PTFE, the photon energy at this wavelength is in the range of the binding energy of the chemical bonds within the polymer. Therefore, even a single photon can cause bond breaking, probably resulting in material removal.

Due to the dominating photo-chemical process, in principle no ablation threshold should be detectable for PMMA at 13.5 nm. This could be confirmed by measuring a substantial material removal also at very low fluences of several

mJ/cm^2 [28]. However, the ablation rate increases rapidly for EUV energy densities above 558 mJ/cm^2. Since the roughness of the ablation profile does not increase with higher energy density, a threshold behavior caused by thermal evaporation or melting can be excluded.

One possible reason for this strong increase of the ablation rate might be the number of chemical bonds which are broken by the incoming EUV photons. At fluences higher than ∼558 mJ/cm^2, this number might exceed a critical number, from where a collective material removal of the polymer fragments becomes possible, whereas for lower fluences, material removal might be a more statistical process.

Additionally, the threshold behavior could also be thermally assisted. Since the fragments need a certain amount of kinetic energy for leaving the surface, a photon-induced increase of the target temperature would accelerate the ablation process.

5 Summary

The EUV induced ablation of the polymers PMMA, PTFE and PC was investigated, employing spectrally pure radiation from a lab-scale source at the wavelength of 13.5 nm. For all three polymers, no incubation behavior could be observed, independent from the EUV energy density. However, the measured ablation rates strongly depend on the polymer type, as well as on the applied EUV fluence. A linear dependence could be detected for low fluences, whereas for higher fluence a logarithmic trend was found. The latter can be described by Lambert–Beer's law, enabling the calculation of ablation thresholds and effective penetration depths. The data were compared and analyzed with respect to the chemical structure of each polymer. For PMMA and PTFE, the effective penetration depths are comparable to tabulated values, indicating a photo-chemical ablation process, where the absorbed photons lead to a strong fragmentation and therefore an emission of small fragments into vacuum. This statement is substantiated by AFM measurements, showing very smooth ablation profiles independent from the incident EUV energy density.

The results were compared to literature data of polymer ablation at higher wavelengths up to 248 nm. It can be concluded that the ablation process at EUV/XUV wavelengths is significantly different from the deep and vacuum UV spectral range (for example PMMA at 248 nm). The main reason is the high photon energy of ∼92 eV, which is nearly one order of magnitude higher than the binding energies within the polymer [30]. The strong fragmentation of the investigated polymers results in very smooth ablation profiles and the absence of an incubation behavior.

Acknowledgements The financial support by the "Deutsche Forschungsgemeinschaft" within the Sonderforschungsbereich 755 "Nanoscale Photonic Imaging" and the collaboration with the Courant Research Centre "Nano-Spectroscopy and X-ray Imaging" is gratefully acknowledged. Furthermore, we thank the COST action MP0601 for organizing fruitful discussions with other researchers working in this field.

References

1. R. Srinivasan, S. Lazare, Polymer **26**, 1297–1300 (1985)
2. S. Küper, S. Modaressi, M. Stuke, J. Phys. Chem. **94**(19), 7514–7518 (1990)
3. R. Srinivasan, J. Appl. Phys. **73**(6), 2743–2750 (1993)
4. J. Ihlemann, K. Rubahn, Appl. Surf. Sci. **154**, 587–592 (2000)
5. T. Lippert, J.T. Dickinson, Chem. Rev. **103** (2003)
6. T. Lippert, Plasma Process. Polym. **2**, 525–546 (2005)
7. D.A. Tichenor, G.D. Kubiak, M.E. Malinowski, R.H. Stulen, S.J. Haney, K.W. Berger, L.A. Brown, R.R. Freeman, W.M. Mansfield, O.R. Wood II, D.M. Tennant, J.E. Bjorkholm, A.A. MacDowell, J. Bokor, T.E. Jewell, D.L. White, D.L. Windt, W.K. Waskiewicz, Opt. Lett. **16**(20), 1557–1559 (1991)
8. L. Juha, M. Bittner, D. Chvostova, J. Krasa, Z. Otcenasek, A.R. Präg, J. Ullschmied, Z. Pientka, J. Krzywinski, J.B. Pelka, A. Wawro, M.E. Grisham, G. Vaschenko, C.S. Menoni, J.J. Rocca, Appl. Phys. Lett. **86**, 034109 (2005)
9. J. Chalupský, Opt. Express **15**, 10 (2007)
10. T. Mocek, B. Rus, M. Stupka, M. Kozlová, A.R. Präg, J. Polan, M. Bittner, R. Sobierajski, L. Juha, Appl. Phys. Lett. **89**, 051501 (2006)
11. M.C.K. Tinone, K. Tanaka, J. Maruyama, N. Ueno, M. Imamura, N. Matsubayashi, J. Chem. Phys. **100**, 5988 (1994)
12. M. Wei, D.T. Attwood, T.K. Gustafson, E.H. Anderson, J. Vac. Sci. Technol. B **12**, 3648 (1994)
13. K. Tanaka, M.C.K. Tinone, H. Ikeura, T. Sekiguchi, T. Sekitani, Rev. Sci. Instrum. **66**, 1474 (1995)
14. Y. Zhang, T. Katoh, M. Washio, H. Yamada, S. Hamada, Appl. Phys. Lett. **67**(6), 865 (1995)
15. M. Inayoshi, M. Ikeda, M. Hori, T. Goto, M. Hiramatsu, A. Hiraya, Jpn. J. Appl. Phys. **34**, L1675 (1995)
16. Y. Zhang, T. Katoh, Jpn. J. Appl. Phys. **35**, L186 (1996)
17. A. Bartnik, H. Fiedorowicz, R. Jarocki, L. Juha, J. Kostecki, R. Rakowski, M. Szczurek, Appl. Phys. B **82**, 529–532 (2006)
18. F. Barkusky, C. Peth, A. Bayer, K. Mann, J. Appl. Phys. **101**(12), 124908 (2007)
19. T. Makimura, Y. Kenmotsu, H. Miyamoto, H. Niino, K. Murakami, Surf. Sci. **593**, 248–251 (2005)
20. F. Barkusky, A. Bayer, C. Peth, K. Mann, Proc. SPIE **6879**, 6879M (2008)
21. S. Kranzusch, K. Mann, Opt. Commun. **200**, 223 (2001)
22. C. Peth, S. Kranzusch, K. Mann, W. Viöl, Rev. Sci. Instrum. **75**(10) 3288 (2004)
23. S. Kranzusch, C. Peth, K. Mann, Rev. Sci. Instrum. **74**(2), 969 (2003)
24. F. Barkusky, C. Peth, K. Mann, T. Feigl, N. Kaiser, Rev. Sci. Instrum. **76**, 105102 (2005)
25. Center for X-Ray Optics, Berkeley Lab, Homepage, http://www-cxro.lbl.gov/ (2011)
26. F. Barkusky, A. Bayer, C. Peth, K. Mann, J. Appl. Phys. **105**, 014906 (2009)

27. F. Barkusky, A. Bayer, S. Döring, P. Grossmann, K. Mann, Opt. Express **18**(5), 4346–4355 (2010)
28. F. Barkusky, C. Peth, A. Bayer, K. Mann, J. Appl. Phys. **101**, 124908 (2007)
29. P.E. Dyer, Appl. Phys. A **77**, 167–173 (2003)
30. C.E. Mortimer, U. Mueller, *Chemie* (Georg Thieme Verlag, Stuttgart, New York, 1987)
31. A. Costela, I. Garcia Moreno, F. Florido, J.M. Figura, R. Sastre, S.M. Hooker, J.S. Cashmore, C.E. Webb, J. Appl. Phys. **77**, 2343 (1995)
32. L. Juha, M. Bittner, D. Chvostova, J. Krasa, Z. Otcenasek, A.R. Präg, J. Ullschmied, Z. Pientka, J. Krzywinski, J.B. Pelka, A. Wawro, M.E. Grisham, G. Vaschenko, C.S. Menoni, J.J. Rocca, Appl. Phys. Lett. **86**, 034109 (2005). 14th International Conference on Vacuum Ultraviolet Radiation Physics, Cairns, Australia, Jul. 19–23, 2004. ISSN 0368–2048
33. D. Riedel, M.C. Castex, Appl. Phys. A, Mater. Sci. Process. **69**(4), 375–380 (1999)
34. S. Küper, M. Stuke, Appl. Phys. Lett. **54**(1), 4–6 (1989)
35. G. Hougham, *Fluoropolymers: Properties* (Springer, Berlin, 1999)
36. M. Lapczyna, M. Stuke, Appl. Phys. A, Mater. Sci. Process. **66**, 473–475 (1998)
37. E. Sutcliffe, E. Srinivasan, Journal of Applied Physics A **60**(9), (1986)
38. B. Braren, Opt. Photonics News **3**(6), 20–23 (1992)
39. A.P. Ghosh, J.E. Hurst, J. Appl. Phys. **64**(1), 287–290 (1988)
40. Y. Tanabe, *Macromolecular Science and Engineering—New Aspects* (Springer, Berlin, 1999)
41. R. Srinivasan, B. Braren, K.G. Casey, J. Appl. Phys. **68**(4), 1842–1847 (1990)
42. S. Küper, M. Stuke, Appl. Phys. A, Mater. Sci. Process. **49**, 211 (1989)